Food and Chemical Toxicology 128 (2019) 202–211

Contents lists available at ScienceDirect

Food and Chemical Toxicology

journal homepage: www.elsevier.com/locate/foodchemtox

# Myclobutanil enantioselective risk assessment in humans through *in vitro* CYP450 reactions: Metabolism and inhibition studies

Franciele S. Fonseca[a], Daniel B. Carrão[a], Nayara C.P. de Albuquerque[a], Viviani Nardini[a], Luís G. Dias[a], Rodrigo M. da Silva[b], Norberto P. Lopes[b], Anderson R.M. de Oliveira[a,*]

[a] Departamento de Química, Faculdade de Filosofia, Ciências e Letras de Ribeirão Preto, Universidade de São Paulo, 14040-901, Ribeirão Preto – SP, Brazil
[b] Núcleo de Pesquisas em Produtos Naturais e Sintéticos, Faculdade de Ciências Farmacêuticas de Ribeirão Preto, Universidade de São Paulo, 14040-903, Ribeirão Preto – SP, Brazil

ARTICLE INFO

*Keywords:*
Myclobutanil
Chiral pesticide
Enantioselective analysis
*In vitro* metabolism
Pesticide-drug interaction

ABSTRACT

Myclobutanil is a chiral triazole fungicide that is employed worldwide. Although enantiomers have the same physical-chemical properties, they may differ in terms of activity, metabolism, and toxicity. This investigation consisted of *in vitro* enantioselective metabolism studies that employed a human model to assess the risks of myclobutanil in humans. A LC-MS/MS enantioselective method was developed and validated. The enzymatic kinetic parameters ($V_{MAX}$, $K_{Mapp}$, and $CL_{INT}$) determined for *in vitro rac*-myclobutanil and *S*-(+)-myclobutanil metabolism revealed enantioselective differences. Furthermore, human CYP450 enzymes did not metabolize *R*-(−)-myclobutanil. The predicted *in vivo* toxicokinetic parameters indicated that *S*-(+)-myclobutanil may be preferentially eliminated by the liver and suffer the first-pass metabolism effect. However, because CYP450 did not metabolize *R*-(−)-myclobutanil, this enantiomer could reach the systemic circulation and stay longer in the human body, potentially causing toxic effects. The CYP450 isoforms CYP2C19 and CYP3A4 were involved in *rac*-myclobutanil and *S*-(+)-myclobutanil metabolism. Although there were differences in the metabolism of the myclobutanil enantiomers, *in vitro* inhibition studies did not show significant enantioselective differences. Overall, the present investigation suggested that myclobutanil moderately inhibits CYP2D6 and CYP2C9 *in vitro* and strongly inhibits CYP3A and CYP2C19 *in vitro*. These results provide useful scientific information for myclobutanil risk assessment in humans.

## 1. Introduction

Myclobutanil (MCL), (*RS*)-2-(4-chlorophenyl)-2-(1H-1,2,4-triazol-1-ylmethyl)hexanenitrile (Fig. 1), is a broad-spectrum systemic triazole fungicide with protective, eradicative, and curative action (University of Hertfordshire, 2018). It is employed to control pests such as powdery mildew, dollar spot, summer patch, rusts, and scab in perennial and annual crops, turf, landscape ornamentals, fruit trees, and vines worldwide (University of Hertfordshire, 2018). Its antifungal activity is related to disrupted fungal membrane function resulting from inhibited sterol biosynthesis (University of Hertfordshire, 2018).

MCL bears an asymmetric carbon, so it is a chiral molecule (Fig. 1). Therefore, there may be significant enantioselective differences in the activities of the MCL racemic mixture and of the isolated MCL enantiomers toward target organisms. The MCL enantiomers have already had their enantioselective antifungal actions evaluated against *Physalospora piricola* (Deng and Hu, 2011), *Gibberella zeae* (Deng and Hu, 2011), *Alternaria kukuchiana* (Deng and Hu, 2011), *Alternaria solani* (Deng and Hu, 2011), *Cercospora arachidicola*, *Fulvia fulva* (Sun et al., 2014), and *Phytophthora infestans* (Sun et al., 2014). For all the evaluated species, (+)-MCL presented higher antifungal activity than (−)-MCL or the racemic mixture (Deng and Hu, 2011; Sun et al., 2014). Notwithstanding the proven differences between the activities of MCL enantiomers, this fungicide is still sold as a racemic mixture.

Significant potential differences among pesticide enantiomers may warrant registration of a single enantiomer product or an enriched mixture of the active enantiomer instead of the racemic mixture (Liu and Tang, 2011). In Switzerland and the Netherlands, pesticides like mecoprop and dichlorprop have been registered as single enantiomer products because the *R*-enantiomers have greater herbicidal activity than the *S*-enantiomers (Liu and Tang, 2011). Replacement of a racemic mixture with a single enantiomer product or an enriched mixture of the

* Corresponding author. Departamento de Química, Faculdade de Filosofia, Ciências e Letras de Ribeirão Preto - USP – Av. dos Bandeirantes, 3900, Ribeirão Preto, São Paulo, 14040-901, Brazil.
*E-mail address:* deoliveira@usp.br (A.R.M. de Oliveira).

https://doi.org/10.1016/j.fct.2019.04.009
Received 14 February 2019; Received in revised form 2 April 2019; Accepted 8 April 2019
Available online 13 April 2019
0278-6915/ 

**Abbreviations**

C – confirmation
CD – circular dichroism
$CL_{INT}$ – *in vitro* intrinsic clearance
$CL_H$ hepatic clearance
$CL'_{INT}$ – *in vivo* intrinsic clearance
CV – coefficient of variation
E – hepatic extraction rate
ECD – electronic circular dichroism
EMA – European Medicines Agency
$f_u$ – unbonded fraction
HLM – human liver microsomes
HQC – high-quality control
IS – internal standard
$IC_{50}$ – half-maximal inhibitory concentration
$K_{Mapp}$ – Apparent Michaelis-Menten constant
LLOQ – lower limit of quantification
LQC – low-quality control
MCL – myclobutanil
MQC – medium-quality control
MRM – multiple reaction monitoring
$NADP^+$ – β-nicotinamide adenine dinucleotide phosphate hydrate
NMF – normal matrix factor
NR – normalized rate
$^Q$ – quantification
R – rotatory strength
RE% – relative error
sTD-DFT – simplified time-dependent density functional theory
ULOQ – upper limit of quantification
$V_0$ – initial velocity
$V_{MAX}$ – maximum velocity
%TNR – total normalized rate

active enantiomer is intended to reduce the amount of pesticide use in the field, consequently lowering the risk of contamination and toxic effects on non-target species, mainly humans (Liu and Tang, 2011).

MCL is moderately toxic to humans (class II) (Sun et al., 2014). It can cause hepatic toxicity, disrupt steroid homeostasis, and affect the reproductive system in animals (Sun et al., 2014). Because MCL persists in the environment, it can accumulate in the food chain, thereby representing a great risk to the human health (Sun et al., 2014). Several papers have reported that MCL residue is present in food (Freeman et al., 2016), water (Zhao et al., 2018), and air (Di Filippo et al., 2018), and MCL has been detected in a controlled baby food simulation study (Kovacova et al., 2014). Therefore, assessing MCL risks in humans is extremely important to provide reliable scientific information regarding the human health (Abass, 2013).

Chiral pesticides may behave with significant enantioselectivity toward non-target organisms, including humans (Drăghici et al., 2013). Therefore, evaluating how MCL interacts with non-target organisms from an enantioselective standpoint is essential to assess its risks (Drăghici et al., 2013). In this sense, MCL toxicity, absorption, distribution, biodegradation, bioaccumulation, and metabolism must be investigated (Drăghici et al., 2013). The toxicity of MCL enantiomers to aquatic algae (*Scenedesmus obliquus*) (Cheng et al., 2013; Li et al., 2015), crustaceans (*Daphnia magna*) (Li et al., 2015), lizards (*Eremias argus*) (Cheng et al., 2017), and zebrafish (*Danio rerio*) (Li et al., 2015) has already been evaluated. These studies demonstrated significant enantioselective differences in MCL toxicity, which varied depending on the evaluated species (Cheng et al., 2017, 2013; Li et al., 2015). MCL biodegradation in strawberry (Zhang et al., 2011), grape (Lin et al., 2018), cucumber (Dong et al., 2012), and soil (Dong et al., 2012) presented significant enantioselective differences, which highlighted risks of contamination and reinforced the importance of conducting enantioselective studies to assess MCL risks.

The *in vitro* enantioselective metabolism of pesticides has been investigated by employing human liver microsomes, which are a reliable resource to perform MCL enantioselective risk assessment in humans (Carrão et al., 2019; de Albuquerque et al., 2018, 2016; Yao et al., 2016). The enantioselective metabolism of a racemic MCL mixture has already been evaluated *in vitro* by using rat liver microsomes (Yan et al., 2014) and rat hepatocytes (Wang et al., 2015). Yan et al. reported significant metabolism differences between MCL enantiomers: the (−)-MCL half-life was more than 10-fold higher than the (+)-MCL half-life, which suggested that rat liver microsomes preferentially degraded (+)-MCL (Yan et al., 2014). Wang et al. also reported significant differences after incubation for 24 h, the (−)-MCL concentration was 1.6 times higher than the (+)-MCL concentration, which suggested that rat hepatocytes preferentially degraded (+)-MCL (Wang et al., 2015).

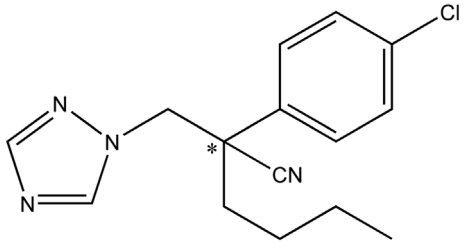


**Fig. 1.** MCL chemical structure. *chiral center.

Hao et al. evaluated the enantioselective MCL absorption, distribution, and metabolism *in vivo* following a single-dose in rats (Hao et al., 2018). Their results suggested preferential (−)-MCL enrichment in the liver, kidney, heart, lung, and testis (Hao et al., 2018). Besides that, (+)-MCL was converted into (−)-MCL in the liver and kidney after 6 h (Hao et al., 2018). Furthermore, the racemic mixture and the individual enantiomers differed both in terms of enrichment and degradation, which suggested enantiomer-specific bioaccumulation (Hao et al., 2018). Finally, five chiral metabolites were detected, and the metabolite pathway was proposed (Hao et al., 2018).

All the aforementioned studies provided reliable scientific information regarding enantioselective MCL metabolism. However, the results could not be correlated because the studies only reported on the relative configuration of the MCL enantiomers. In addition, the studies employed rat as models. Because interspecies differences in enantioselective MCL metabolism may exist, predicting risk assessment in humans requires that enantioselective MCL metabolism be evaluated by using a human model.

In this scenario, the present work aimed to evaluate the enantioselective MCL metabolism and CYP450 inhibitory potential *in vitro* by investigating a MCL racemic mixture and its individual enantiomers in a human model. For the first time, the enzymatic kinetic parameters of *in vitro* MCL metabolism have been characterized, the main CYP450 enzymes responsible for MCL metabolism have been determined, the *in vivo* toxicokinetic parameters have been predicted, and the MCL inhibitory potential over the main CYP450 enzymes has been investigated to predict pesticide-drug interactions.

## 2. Materials and methods

### 2.1. Chemicals and reagents

*Rac*-myclobutanil (≥99.4%) was acquired from Sigma-Aldrich (St. Louis, MO, USA). The standard *rac*-MCL stock solution was prepared at 4000 μmol $L^{-1}$ in methanol. The probe substrates and their metabolites

(markers) phenacetin (≥98.0%), acetaminophen (≥98.0%), diclofenac (≥98.0%), chlorzoxazone (≥98%), and nifedipine (≥98%) were purchased from Sigma-Aldrich (St. Louis, MO, USA); 4′-hydroxy diclofenac (≥98.0%), S-mephenytoin (≥98.0%), 4′-hydroxy mephenytoin (≥98.0%), bufuralol (≥98.0%), 1′-hydroxy bufuralol (≥98.0%), 6-hydroxychlorzoxazone (≥98%), and dehydronifedipine (≥98%) were obtained from Toronto Research Chemicals (Toronto, Canada); and midazolam (≥98%) as well as 1-hydroxymidazolam (≥95%) were acquired from Cayman Chemicals (Ann Arbor, MI, USA). The standard stock solutions of the probe substrates were prepared at the following concentrations and in the following solvents: phenacetin (962 μmol $L^{-1}$, acetonitrile), diclofenac (3956 μmol $L^{-1}$, methanol), S-mephenytoin (8000 μmol $L^{-1}$, acetonitrile), bufuralol (432 μmol $L^{-1}$, acetonitrile), chlorzoxazone (11672 μmol $L^{-1}$, acetonitrile), midazolam (433 μmol $L^{-1}$, acetonitrile), and nifedipine (560 μmol $L^{-1}$, acetonitrile). The standard stock solutions of the metabolites were prepared at 1000 μmol $L^{-1}$ in the same solvents as the respective substrate. Diazepam (99.2%), tolbutamide (≥97.0%), and bisphenol A-d16 (≥98%), which were employed as internal standard (IS), were acquired from Sigma-Aldrich (St. Louis, MO, USA). The IS stock solutions were prepared at 1 μmol $L^{-1}$ in methanol. All the standard solutions were stored in amber tubes at −20 °C.

Human liver microsomes (HLMs), pooled from 150 donors, and CYP450 recombinant isoforms (Supersomes®) were purchased from Corning Life Science (Phoenix, AZ, USA) and stored at −80 °C. Ultrapure water was obtained from a Direct-Q 3 Milli-Q system from Millipore (Billerica, MA, USA). Methanol, ethanol, hexane, isopropanol, chloroform, and ethyl acetate (HPLC grade) were acquired from Panreac (Barcelona, Spain). The analytical grade reagents sodium dihydrogen phosphate, sodium hydrogen phosphate dihydrate, and formic acid were obtained from Synth (Diadema, Brazil); tris(hydroxymethyl)aminomethane was acquired from J. T. Baker (Philipsburg, MT, USA); potassium chloride was purchased from Mallinckrodt Chemicals (Xalostoc, Mexico); and β-nicotinamide adenine dinucleotide phosphate hydrate ($NADP^+$), glucose-6-phosphate, glucose-6-phosphate dehydrogenase, and macrogol glycerol ricinoleate (Cremophor EL®) were acquired from Sigma-Aldrich (St. Louis, MO, USA).

### 2.2. MCL isolation and optical rotation sign and absolute configuration determination

The MCL enantiomers were isolated in a Shimadzu HPLC system (Kyoto, Japan) consisting of two LC-6AD solvent pump units, an SCL-10AVP controller system, and an SPD-10AV diode array detector. The enantiomers were isolated at room temperature (23 ± 2 °C). A Chiralpak AD-H® column (150 × 4.6 mm, 5 μm) was employed. Methanol at a flow rate of 0.3 mL $min^{-1}$ was used as mobile phase. The enantiomers were detected at 223 nm. The isolated enantiomers were stored in amber tubes at −20 °C.

The isolated MCL enantiomers had the optical rotation sign determined on a J-810 circular dichroism spectropolarimeter (Jasco, Tokyo, Japan). The enantiomers were solubilized in methanol, and the spectrum (four accumulated scans) was recorded from 210 to 300 nm after correction with a blank solution (methanol). The analyses were performed at 25 °C; a cell with a path length of 1 mm was employed.

### 2.3. Conformational analysis and electronic circular dichroism calculations

The conformational search was conducted with VegaZZ release 3.1.1.42 (Pedretti et al., 2004, 2003, 2002). A systematic scan was carried out on the flexible dihedrals with optimization in the MMFF94 force field at each angle step. After the conformational search, the set of conformers for the *R*-MCL and *S*-MCL enantiomers was subjected to local geometry optimizations at the DFT level. All the quantum calculations were accomplished with ORCA4.0.1.2 (Neese, 2012). A detailed description regarding the conformational analysis can be found in the Supplementary material section.

### 2.4. LC-MS/MS conditions for the enantioselective analysis

The enantioselective analysis of myclobutanil was performed on a Prominence HPLC system (Shimadzu, Kyoto, Japan) consisting of a LC-20AD solvent pump unit, a DGU-20A3R online degasser, a SIL-20ACHT automatic injector, a CTO-20AC column oven, and a CBM-20A controller system coupled to an API 3200 triple quadrupole mass spectrometer (AB Sciex, Toronto, Canada) equipped with an ESI interface, operating in positive mode. The analysis was conducted by employing a Chiralpak AD-H® analytical column (150 × 4.6 mm, 5 μm) and an Ascentis Express $C_{18}$ (3.0 mm × 4.6 mm, 2.7 μm) guard column (Supelco, Bellefonte, PA, USA). The mobile phase consisted of 0.1% formic acid in methanol at a flow rate of 0.9 mL $min^{-1}$. The analysis was carried out at 35 °C, and the injection volume was 10 μL. Multiple reaction monitoring (MRM) transitions were monitored, and the reactions used for quantification ($^Q$) and confirmation ($^C$) were *m/z* 289.1 → 70.0$^Q$ and 289.1 → 125.2$^C$ for MCL enantiomers and *m/z* 285.1 → 193.1$^Q$ and 285.1 → 154.1$^C$ for IS. The collision energy was set at 35 eV. The nebulizer, turbo, and collision pressures were 50, 40, and 4 psi, respectively. The capillary voltage and the drying temperature were 5000 V and 700 °C, respectively. Data were collected and analyzed with the aid of Analyst software, version 1.5.2 (Ontario, Canada).

### 2.5. Microsomal incubation conditions

The microsomal medium consisted of MCL (*rac*-MCL, *S*-(+)-MCL, or *R*-(−)-MCL), NADPH regeneration solution, HLMs, and phosphate buffer solution (0.1 mol $L^{-1}$; pH 7.4) with 0.25% (m/v) Cremophor EL® at a final volume of 200 μL. The NADPH regeneration solution comprised glucose-6-phosphate (5.0 mmol $L^{-1}$), β-nicotinamide adenine dinucleotide phosphate sodium (0.25 mmol $L^{-1}$), and glucose-6-phosphate dehydrogenase (0.4 units $mL^{-1}$) in tris-KCl buffer [tris(hydroxymethyl)aminomethane 0.05 mol $L^{-1}$ and KCl 0.15 mol $L^{-1}$; pH 7.4). After pre-warming for 5 min in a shaking water bath at 37 °C, the metabolism reaction was initiated by addition of the NADPH regeneration solution. The initial velocity ($V_0$) conditions were determined in the linear range according to the incubation time and to the microsomal protein content for the *rac*-MCL depletion from the medium. The metabolism reactions were stopped by addition of 600 μL of ethyl acetate to the microsomal incubation medium. After that, the samples were shaken at 1000 rpm in a Vibrax VXR agitator (IKA, Staufen, Germany) for 10 min and centrifuged at 1800 × *g* in a HIMAC CF16RXII centrifuge (Hitachi, Tokyo, Japan) for 10 min. Then, the organic phase was collected and evaporated by employing a Concentrator Plus Speed Vacuum (Eppendorf, Hamburg, Germany). Finally, the residue was solubilized in 200 μL of mobile phase and analyzed.

### 2.6. Bioanalytical Method Validation

The bioanalytical method was validated; the following parameters were considered: selectivity, linearity, carryover, lower limit of quantification, accuracy, precision, matrix effect, and stability. The acceptance criteria were based on the "Guideline on Bioanalytical Method Validation" by the European Medicines Agency (EMA) (EMA, 2012). Linearity (n = 3) was evaluated for each MCL enantiomer. Two analytical curves, named "low range" and "high range", were used: the low range included 0.025, 0.050, 0.38, 0.50, 1.25, 1.56, and 2.49 μmol $L^{-1}$; the high range included 2.49, 3.74, 7.47, 9.96, 19.91, 31.55, and 49.78 μmol $L^{-1}$. The analytical curves were constructed by plotting the MCL/IS peak area ratio *versus* the MCL enantiomer concentration. As the residual analysis of the analytical curves showed heteroscedastic behavior, a weighting factor ($1/x^2$) was applied to ensure linearity.

The selectivity of the method was examined by analyzing HLM blank samples (without MCL or the IS). Carryover was evaluated by

analyzing HLM blank samples after a sample at the upper limit of quantification (ULOQ) was analyzed. Accuracy and precision, within-run (n = 5) and between-run (n = 3), were assessed for the lowest limit of quantification (LLOQ) and for the low- (LQC), medium- (MQC), and high-quality control (HQC) samples of each MCL enantiomer. Accuracy was expressed as the relative error (RE%), and precision was expressed as the coefficient of variation (CV). The limits of accuracy and precision were set at ± 15% for the LQC, MQC, and HQC samples and at ± 20% for the LLOQ samples.

The matrix effect was evaluated by analyzing (i) blank HLM samples spiked (after the sample preparation procedure) with *rac*-MCL and IS or (ii) pure *rac*-MCL and IS solutions (methanol). The determination was performed for the LQC and HQC samples in both analytical curve ranges. The normalized matrix factor (NMF) was calculated as the ratio of the MCL/IS peak areas from (i) and (ii) of each enantiomer. The NMF limit for the coefficient of variation was set at 15%.

The MCL stability (n = 5) was assessed (i) at incubation conditions (40 min at 37 °C) and (ii) in the autosampler (24 h at 25 ± 2 °C) at two concentration levels (LQC and HQC). The sample stabilities were determined by using fresh analytical curves prepared on the same day. Each MCL enantiomer concentration at each sample stability should be within ± 15% of the nominal concentration.

### 2.7. Determining enzymatic kinetic parameters

The enzymatic parameters for MCL metabolism were individually determined for *rac*-MCL, *S*-(+)-MCL, and *R*-(−)-MCL. For this analysis, the enzymatic kinetic studies were conducted at $V_0$ conditions by employing a microsomal protein concentration of 0.5 mg mL$^{-1}$ and incubation time of 50 min. The metabolism incubations involved substrate concentrations ranging from 0.10 to 50.00 μmol L$^{-1}$ (n = 3). The remaining *rac*-MCL, *S*-(+)-MCL, and/or *R*-(−)-MCL concentrations were determined by using analytical curves prepared on the same day, and the metabolized concentrations were calculated. The enzymatic parameters ($K_{Mapp}$ and $V_{MAX}$) were obtained by nonlinear regression analysis carried out with GraphPad Prism Software 5.00 (San Diego, CA, USA), and the *in vitro* intrinsic clearance ($CL_{INT}$) was calculated according to Seibert and Tracy (2014) (Seibert and Tracy, 2014).

### 2.8. Predicting in vivo toxicokinetic parameters

The percentage of MCL bound to microsomal and plasmatic proteins was determined by employing *rac*-MCL, *S*-(+)-MCL, or *R*-(−)-MCL at a concentration corresponding to the determined $K_{Mapp}$ (n = 3). To determine binding to microsomal proteins, MCL was incubated with HLMs (microsomal protein concentration of 0.5 mg mL$^{-1}$) in the absence of NADPH regeneration solution. To determine binding to plasmatic proteins, MCL was incubated with human plasma (plasmatic protein concentration of 42 mg mL$^{-1}$) in phosphate buffer solution (pH 7.4, 0.1 mol L$^{-1}$) (Chang et al., 2010). Control samples without microsomal or plasmatic proteins were simultaneously prepared. After incubation at 37 °C for 10 min, the samples were placed in a 30 kDa Amicon ultra centrifugal filter device (Millipore Corporation, Bedford, MA, USA) and centrifuged at 10,000 × *g* (Hitachi CF16RXII, Himac, Tokyo, Japan) for 20 min. The ultrafiltrates were diluted with methanol, and the samples were analyzed by LC-MS/MS. The unbound fraction ($f_u$) was determined by using the ratio between the concentrations of the sample and the control (Giuliano et al., 2005). The $CL_{INT}$ was scaled to *in vivo* intrinsic clearance ($CL'_{INT}$) by employing a scaling factor of 40 mg of microsomal protein/g of liver and 21.4 g of liver/kg of bodyweight (Bowman and Benet, 2018). The hepatic clearance ($CL_H$) (Equation (1)) and the hepatic extraction rate (E) (Equation (2)) were calculated (Bowman and Benet, 2018).

$$CL_H = \frac{Q\ x\ \frac{f_{u,plasm}}{f_{u,mic}}\ x\ CL'_{INT}}{Q + (\frac{f_{u,plasm}}{f_{u,mic}}\ x\ CL'_{INT})} \quad (1)$$

where $CL_H$ is the hepatic clearance, $f_{u,plasm}$ is the fraction of substrate unbound to plasmatic proteins, $f_{u,mic}$ is the fraction of substrate unbound to microsomal proteins, $CL'_{INT}$ is the *in vivo* intrinsic clearance, and Q is the hepatic blood flow (20 mL min$^{-1}$ kg$^{-1}$) (Damre and Iyer, 2012).

$$E = \frac{\frac{f_{u,plasm}}{f_{u,mic}}\ x\ CL'_{INT}}{Q + (\frac{f_{u,plasm}}{f_{u,mic}}\ x\ CL'_{INT})}\ x\ 100\% \quad (2)$$

where E is the hepatic extraction rate, $f_{u,plasm}$ is the fraction of substrate unbound to plasmatic proteins, $f_{u,mic}$ is the fraction of substrate unbound to microsomal proteins, $CL'_{INT}$ is the *in vivo* intrinsic clearance, and Q is the hepatic blood flow (20 mL min$^{-1}$ kg$^{-1}$) (Damre and Iyer, 2012).

### 2.9. CYP450 reaction phenotyping

To determine which CYP isoform(s) was (were) involved in MCL (*rac*-MCL, *S*-(+)-MCL, or *R*-(−)-MCL) metabolism, MCL was incubated with each of the following CYP450 recombinant isoforms at a concentration corresponding to the determined $K_{Mapp}$ (n = 3): rCYP1A1, rCYP1A2, rCYP3A4, rCYP3A5, rCYP2B6, rCYP2C8, rCYP2C9, rCYP2C19, rCYP2D6, and rCYP2E1. The medium consisted of MCL (*rac*-MCL, *S*-(+)-MCL, or *R*-(−)-MCL), rCYP450 (50 pmol mL$^{-1}$), NADPH regeneration solution (0.25 mmol L$^{-1}$ $NADP^+$, 5.0 mmol L$^{-1}$ D-glucose-6-phosphate, and 0.4 UmL$^{-1}$ glucose-6-phosphate dehydrogenase), and phosphate buffer (0.1 mol L$^{-1}$; pH 7.4) with 0.25% (m/v) Cremophor EL® at a final volume of 200 μL. A control sample, composed of insect control Supersomes® instead of CYP450 recombinant isoforms, was analyzed simultaneously for comparison purposes. The reactions were started by addition of the NADPH regeneration solution after pre-warming for 5 min. After 50 min, the reactions were stopped when the sample preparation procedure was initiated. The results are expressed as a percentage of the total normalized rate (%TNR), by using the method described by Rodrigues (1999). Briefly, the MCL depletion rate was multiplied by the abundance of each CYP in the native human liver microsome, to obtain a normalized rate (NR). The NRs for each CYP involved in MCL depletion were summed to obtain the total normalized rate (TNR). The NR of each CYP was expressed as a percentage of the TNR (Rodrigues, 1999). The results were analyzed by using GraphPad Prism Software 5.00 (San Diego, CA, USA).

### 2.10. CYP450 inhibition studies

The inhibitory potential of CYP450 isoforms by MCL was evaluated by using human liver microsomes. To this end, each CYP isoform metabolism rate was compared in the presence and absence of the pesticide, and the MCL half-maximal inhibitory concentration ($IC_{50}$) was determined. To assess stereoselectivity during inhibition of the CYP450 isoforms, the assays were performed by using the MCL racemic mixture of or each single enantiomer (*S*-(+)-MCL or *R*-(−)-MCL).

This study employed a probe substrate that was specific for each evaluated CYP isoform. The probe substrates (and their concentrations) in the microsomal medium (volume of 400 μL) were: phenacetin (12.03 μmol L$^{-1}$) for CYP1A2, diclofenac (49.45 μmol L$^{-1}$) for CYP2C9, S-mephenytoin (44.83 μmol L$^{-1}$) for CYP2C19, bufuralol (5.40 μmol L$^{-1}$) for CYP2D6, chlorzoxazone (145.90 μmol L$^{-1}$) for CYP2E1, and midazolam (5.41 μmol L$^{-1}$) and nifedipine (7.00 μmol L$^{-1}$) for CYP3A4/5. The incubation conditions for the inhibitory assay, including the human liver microsomal protein

concentration and the incubation time, were previously determined by (Habenschus et al., 2017) and are summarized in Table 1. MCL was used at seven concentration levels, from 0.01 to 100.00 μmol $L^{-1}$, in microsomal medium. Moreover, the controls were conducted in the absence of MCL. Positive controls for all the CYP450 isoforms were also analyzed by using selective inhibitors for each CYP450 as described by (Habenschus et al., 2017). All the experiments were carried out in triplicate.

The microsomal medium consisted of MCL (*rac*-MCL, *S*-(+)-MCL or *R*-(−)-MCL), probe substrate, HLM, NADPH regeneration solution (0.25 mmol $L^{-1}$ $NADP^+$, 5.0 mmol $L^{-1}$ D-glucose-6-phosphate, and 0.4 U $mL^{-1}$ glucose-6-phosphate dehydrogenase), and phosphate buffer (0.1 mol $L^{-1}$, pH 7.4) at a final volume of 400 μL. The microsomal medium was pre-warmed in a water-shaking bath at 37 °C for 5 min, and the reaction was started by addition of the NADPH regeneration solution. After incubation (Table 1), the reaction was stopped by addition of 1.0 mL of organic solvent, followed by addition of the modifier, when necessary, and the internal standard solution (Table 1). Then, the samples were shaken in a Vibrax VXR agitator (IKA, Wilmington, NC, USA) at 1000 rpm for 15 min and centrifuged at 1800 × *g* for 10 min in a HIMAC CF16RXII centrifuge (Hitachi, Tokyo, Japan). The organic phase was collected and dried with the aid of a Concentrator Plus speed vacuum (Eppendorf, Hamburg, Germany). The residues were solubilized in 200 μL of mobile phase and analyzed. All the CYP450 isoforms were analyzed by employing the previously described LC-MS/MS (see Supplementary material). To determine the MCL $IC_{50}$ value, a nonlinear regression of the percentage of the remaining enzymatic activity (Equation (3)) of each CYP450 isoform evaluated against the logarithm of the MCL concentration in the microsomal medium was fitted; the GraphPad Prism Software 5.00 (San Diego, CA, USA) was used.

$$\%REA = \frac{A_i}{A_0 . 100} \quad (3)$$

Where: % REA corresponds to the percentage of remaining enzymatic activity, Ai corresponds to the area of the metabolite formed when the incubation was performed with the standard substrate and myclobutanil, and $A_0$ corresponds to the area of the metabolite formed when the incubation was performed with the standard substrate in the absence of myclobutanil.

## 3. Results and discussion

### 3.1. Optical rotation sign and absolute configuration determination

The optical rotation sign of MCL enantiomers was established by employing circular dichroism (CD). At 223 nm, the first and the second MCL enantiomer to elute (E1 and E2, respectively) showed a positive and a negative Cotton effect, respectively (Figs S1 and S2, respectively). Thus, E1 was (+)-MCL, whereas E2 was (−)-MCL. The MCL absolute configuration was determined by ECD calculations. The most stable and the five most stable conformers of each enantiomer were used in the calculations (the first five conformers totaled approximately 50% of the conformer population of each enantiomer). For comparison with the experimental spectra, the standard deviations of the Gaussian-shaped curves were replaced with only one parameter (σ). There were no statistically significant differences between the ECD spectra calculated for the most stable and the five most stable conformers. Fig S3-6 show the theoretical ECD results of the most stable and the five most stable *S*-MCL and *R*-MCL conformers. Fig S7contains a representation of the five first most stable *S*-MCL and *R*-MCL conformers. Table S1 lists the absorption wavelength and the optical rotatory strength for the most stable *S*-MCL and *R*-MCL conformers in the range of 190 nm–250 nm. The *S*-MCL theoretical ECD presented a positive Cotton effect, whereas the theoretical *R*-MCL ECD evidenced a negative Cotton effect. Therefore, the first and the second MCL enantiomer to elute (E1 and E2, respectively) were identified as *S*-(+)-MCL and *R*-(−)-MCL, respectively.

### 3.2. Bioanalytical Method Validation

The bioanalytical method was successfully validated. The method was selective as judged from the absence of interference peaks in the *S*-(+)-MCL, *R*-(−)-MCL, or IS retention times (Fig S8). Because an extensive range of concentrations was necessary, two analytical curves were prepared to quantify each MCL enantiomer, the “low-range curve” from 0.025 to 2.49 μmol $L^{-1}$, and the “high-range curve” from 2.49 to 49.78 μmol $L^{-1}$. The linearity (n = 3) of both analytical curves constructed for *S*-(+)-MCL and *R*-(−)-MCL was suitable—the correlation coefficient was higher than 0.99, and the relative error (RE%) was below 15% for each concentration. In addition, the residual plot revealed normal distribution of random errors (Fig S9). Table S2 brings the linear equation and the correlation coefficients. There was no carryover effect (data not shown). The LLOQ of the analytical method was 0.025 μmol $L^{-1}$ for the low-range curve and 2.49 μmol $L^{-1}$ for the high-range curve for each MCL enantiomer, with RE% and CV values lower than 10% and 15%, respectively. Table S3 summarizes the within -run and the between-run accuracy and precision. Neither RE% nor CV exceeded a value of 14%. Table S4 presents the matrix effect results, expressed as NMF, with CV values less than 15%. The stability tests showed that the MCL enantiomers remained stable at all the evaluated concentrations and conditions (Table S5).

### 3.3. Determining enzymatic kinetic parameters

The enzymatic kinetics of enantioselective MCL metabolism by HLMs was evaluated in $V_0$ conditions according to the incubation time (50 min) and the microsomal protein content (0.5 mg protein $mL^{-1}$). The kinetics of *rac*-MCL incubation with HLMs was plotted by monitoring both the *S*-(+)-MCL and the *R*-(−)-MCL concentration, individually. A significant enantioselective difference emerged when *rac*-MCL was incubated with HLMs. *S*-(+)-MCL was metabolized by CYP450 enzymes, whereas *R*-(−)-MCL was not. Therefore, regarding *rac*-MCL incubation with HLMs, only the enzymatic kinetics related to

**Table 1**
Experimental conditions and sample preparation procedure for CYP450 inhibition assay with human liver microsomes.

| CYP450 isoform | Marker reaction | Microsomal protein (mg $mL^{-1}$) | Incubation time (min) | Internal standard | Organic Solvent |
|---|---|---|---|---|---|
| CYP1A2 | Phenacetin O-deethylation | 0.30 | 30 | Diazepam | Ethyl acetate |
| CYP2C9 | Diclofenac 4′-hydroxylation | 0.10 | 20 | Diazepam | Chloroform[a] |
| CYP2C19 | S-mephenytoin 4′-hydroxylation | 0.20 | 60 | Bisphenol A-d16 | Ethyl acetate |
| CYP2D6 | Bufuralol 1′-hydroxylation | 0.25 | 30 | Diazepam | Ethyl acetate[b] |
| CYP2E1 | Chlorzoxazone 6-hydroxylation | 0.40 | 20 | Tolbutamide | Chloroform |
| CYP3A4/5 | Midazolam 1-hydroxylation | 0.10 | 10 | Diazepam | Ethyl acetate |
| CYP3A4/5 | Nifedipine oxidation | 0.15 | 15 | Diazepam | Ethyl acetate[c] |

Modifier: (a) 100 μL HCl 1.2 mol $L^{-1}$, (b) 100 μL NaOH 4 mol $L^{-1}$, 100 μL NaOH 1 mol $L^{-1}$.
CYP450 - cytochrome P450.

*S*-(+)-MCL metabolism by CYP450 enzymes could be plotted (Fig. 2A). The plot of *rac*-MCL metabolism by HLMs indicated Michaelis-Menten kinetic behavior, which was confirmed by an Eadie-Hofstee plot. Enzymatic kinetic studies were also performed by incubating *S*-(+)-MCL and *R*-(−)-MCL individually with HLMs. The *S*-(+)-MCL metabolism enzymatic kinetic profile also indicated Michaelis-Menten kinetic behavior (Fig. 2B), which was also confirmed by an Eadie-Hofstee plot. However, once again, it was not possible to determine the enzymatic kinetic profile for *R*-(−)-MCL metabolism by HLMs because human CYP450 enzymes did not metabolize this enantiomer. Table 2 lists the enantioselective enzymatic parameters ($K_{Mapp}$, $V_{MAX}$) determined after MCL metabolism by HLMs *in vitro*. The kinetic parameters obtained from *S*-(+)-MCL incubation showed higher $V_{MAX}$ and $K_{Mapp}$ values as compared to *rac*-MCL incubation (Table 2). The lower values obtained for *rac*-MCL incubation might be associated with *S*-(+)-MCL metabolism inhibition by CYP450 enzymes elicited by *R*-(−)-MCL. In a study employing rat liver microsomes (RLMs), Yan et al. (2014) reported that MCL degradation was stereoselective: (+)-MCL was degraded 11.3-fold faster than (−)-MCL. Differences between MCL enantiomers in terms of enzymatic kinetic parameters were also reported. The (+)-MCL $V_{MAX}$ was fourfold the (−)-MCL $V_{MAX}$ (Yan et al., 2014). In contrast, both MCL enantiomers were metabolized when RLMs were employed, as opposed to only *S*-(+)-MCL being metabolized in the presence of HLMs. These differences between species highlighted the importance of employing human models to assess the risk of exposure to chiral pesticides as judged from the significant enantioselective differences that have been observed (Martignoni et al., 2006). Intrinsic clearance ($CL_{INT}$), which is the capacity of liver enzymes to eliminate a chemical according to the blood flow rate and to protein binding (Seibert and Tracy, 2014), was 2.5 times higher for *S*-(+)-MCL than for *rac*-MCL. This indicated that *S*-(+)-MCL metabolism in the presence or absence of *R*-(−)-MCL was significantly enantioselective. $CL_{INT}$ does not reflect pesticide elimination from the body.

### 3.4. Predicting in vivo toxicokinetic parameters

To extrapolate the results obtained *in vitro* to *in vivo* toxicokinetic parameters, nonspecific binding to plasmatic and microsomal proteins and hepatic blood flow should be considered (Chang et al., 2010). Therefore, the MCL fraction unbound to microsomal and plasmatic proteins was determined for *rac*-MCL, *S*-(+)-MCL, and *R*-(−)-MCL, individually. For *rac*-MCL incubation, the *S*-(+)-MCL fraction unbound to microsomal protein ($f_{u,mic}$) and to plasmatic proteins ($f_{u,plasm}$) was 0.73 and 0.17, respectively. As for *R*-(−)-MCL, $f_{u,mic}$ and $f_{u,plasm}$ were 0.66 and 0.10, respectively. For individual *S*-(+)-MCL incubation, $f_{u,mic}$ and $f_{u,plasm}$ were 0.83 and 0.18, respectively. Finally, for *R*-(−)-MCL, $f_{u,mic}$ and $f_{u,plasm}$ were 0.90 and 0.12, respectively. By considering the results of enantioselective MCL nonspecific binding to plasmatic and microsomal proteins and a hepatic blood flow of 20 mL $min^{-1}$ $kg^{-1}$ (Damre and Iyer, 2012), the hepatic clearance ($CL_H$) and the hepatic extraction ratio (E) were predicted (Table 2). Extrapolation for *R*-(−)-MCL incubation was not performed because CYP450 enzymes did not metabolize *R*-(−)-MCL, as described above. The $CL_H$ values for *rac*-MCL and *S*-(+)-MCL were close to 20 mL $min^{-1}$ $kg^{-1}$ (which was equivalent to the hepatic blood flow). This meant that *S*-(+)-MCL could preferentially be eliminated by the liver (Damre and Iyer, 2012). In addition, the hepatic extraction ratio close to 100% for *rac*-MCL and *S*-(+)-MCL indicated that *S*-(+)-MCL could suffer the first-pass metabolism effect by the liver (Coleman, 2006).

These results pointed out that, in case of human contamination by MCL, the *S*-(+)-MCL concentration should be significantly decreased before this enantiomer reaches the systemic circulation because it could suffer the first-pass metabolism effect in the liver. However, since CYP450 enzymes do not metabolize *R*-MCL, the latter could reach the systemic circulation, thereby staying longer in the human body and potentially causing toxic effects. The results obtained herein attested to an extreme difference in the *in vitro* enantioselective metabolism of MCL enantiomers by HLMs and highlighted the importance of employing human models to evaluate the enantioselective metabolism of chiral pesticides.

In the studies performed by Deng and Hu, (+)-MCL presented higher fungicidal activity than (−)-MCL against *Physalospora piricola*, *Gibberella zeae*, *Alternaria kukuchiana*, and *Alternaria solani* (Deng and Hu, 2011). However, herein, the absolute configuration of the MCL enantiomers was not determined, which prevented us from correlating the aforementioned results with the results obtained in the present work. To determine which enantiomer has higher fungicidal activity and to correlate the results with extrapolated *in vivo* toxicokinetic parameters in humans, the use of MCL as a pure enantiomer or as an enriched mixture must be proposed (Basheer, 2018). As a consequence, the amount of employed pesticide could be lower, reducing the risk of environmental contamination and human exposure (Basheer, 2018).

### 3.5. CYP450 reaction phenotyping

To determine the human CYP450 isoforms involved in MCL enantiomer metabolism, a study employing CYP450 recombinant isoforms was carried out. The major isoforms involved in xenobiotic metabolism (Ogilvie et al., 2008) were evaluated: rCYP1A1, rCYP1A2, rCYP3A4, rCYP3A5, rCYP2B6, rCYP2C8, rCYP2C9, rCYP2C19, rCYP2D6, and rCYP2E1. The %TNR of each isoform for *rac*-MCL and *S*-(+)-MCL metabolism was calculated (Fig. 3).

The main isoforms involved in *S*-(+)-MCL metabolism, determined by employing *rac*-MCL and the isolated enantiomer *S*-(+)-MCL, were CYP2C19 and CYP3A4. When *rac*-MCL was used as the substrate, the %TNR was 57.9% for CYP2C19 and 42.1% for CYP3A4. In the case of *S*-(+)-MCL metabolism, the %TNR was 43.3% for CYP2C19 and 56.7% for CYP3A4. A major contribution of CYP2C19 to *S*-(+)-MCL was

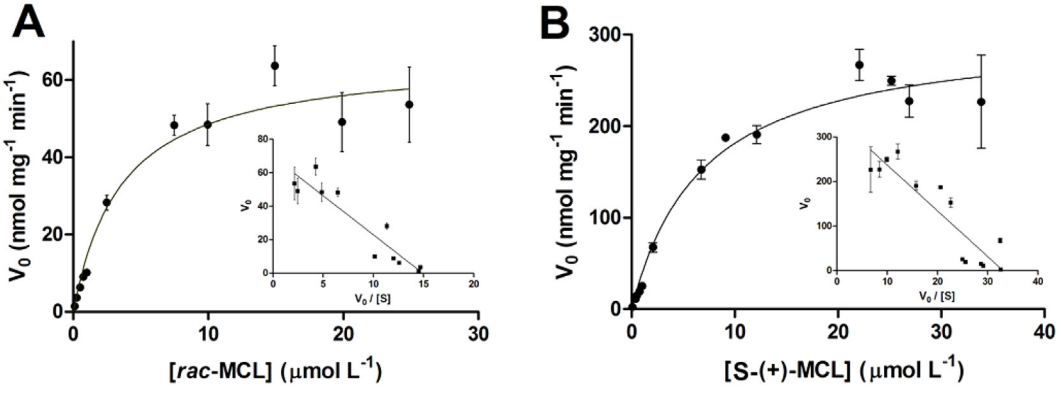


**Fig. 2.** Enzymatic kinetics for (A) *rac*-MCL and (B) *S*-(+)-MCL after *in vitro* metabolism by human liver microsomes. Inside, smaller: the Eadie-Hofstee plot.

**Table 2**
Enantioselective *in vitro* enzymatic kinetic parameters and predicted *in vivo* toxicokinetic parameters for *rac*-MCL, *S*-(+)-MCL, and *R*-(−)-MCL metabolism.

| Substrate | Monitoring | $K_{Mapp}$ (μmol $L^{-1}$) | $V_{MAX}$ (nmol $min^{-1}$ $mg^{-1}$) | $CL_{INT}$ (mL $min^{-1}$ $mg^{-1}$) | $CL_H$ (mL $min^{-1}$ $kg^{-1}$) | E (%) |
|---|---|---|---|---|---|---|
| *rac*-MCL | *S*-(+)-MCL | 3.6 ± 0.9 | 66.1 ± 4.6 | 18.3 ± 4.6 | 19.89 | 99.5 |
| | *R*-(−)-MCL | – | – | – | – | – |
| *S*-(+)-MCL | *S*-(+)-MCL | 6.8 ± 1.3 | 305.5 ± 18.4 | 44.6 ± 8.8 | 19.95 | 99.8 |
| *R*-(−)-MCL | *R*-(−)-MCL | – | – | – | – | – |

$K_{Mapp}$ - apparent Michaelis-Menten constant.
$V_{MAX}$ - maximum velocity.
$CL_{INT}$ - *in vitro* intrinsic clearance.
$CL_H$ - hepatic clearance.
E − hepatic extraction rate.
MCL - myclobutanil.

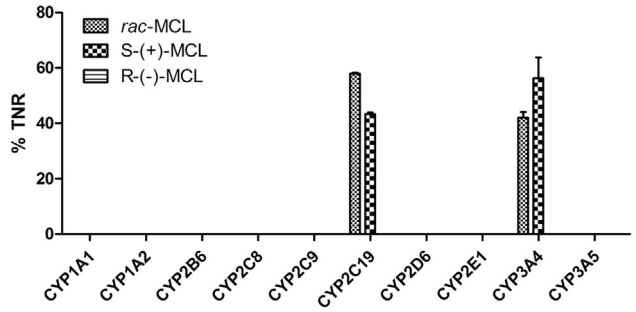


**Fig. 3.** Human CYP450 isoforms involved in *rac*-MCL, *S*-(+)-MCL, and *R*-(−)-MCL metabolism.

observed when *rac*-MCL was the substrate. When *S*-(+)-MCL was used as the substrate, CYP3A4 had a major contribution. This fact can be attributed to CYP3A4 inhibition by *R*-(−)-MCL. CYP3A4 is known to be the major isoform underlying the metabolism of *trans*-bromuconazole, another triazole fungicide (Mazur et al., 2007), and CYP2C19 has been reported to be involved in the metabolism of several pesticides, such as deltamethrin and esfenvalerate (Godin et al., 2007). In the nonchiral study performed by Barton et al. (2006), these authors employed human recombinant isoforms and reported that the CYP2C and CYP3A subfamilies were the major isoforms responsible for MCL metabolism, in agreement with the results obtained in the present work. In addition, once again, the results of the present work indicated that CYP450 recombinant isoforms did not significantly metabolize *R*-(−)-MCL, pointing to an enantioselective difference in MCL enantiomer metabolism by human CYP450 enzymes.

### 3.6. CYP450 inhibition studies

The CYP450 enzymes underlying MCL metabolism are also the main enzymes involved in the metabolism of several drugs (Sychev et al., 2018). For this reason, drug-pesticide interactions may occur due to inhibition of CYP450 metabolic activities or induction of their expression (Abass and Pelkonen, 2013). These interactions affect drug plasma concentrations and may result in loss of pharmacological activity or even overdose (Abass and Pelkonen, 2013). Most drug-drug or drug-xenobiotic interactions originate from inhibited metabolism (Ring et al., 2014). For this reason, evaluating how/whether pesticides inhibit CYP450 enzymes is extremely important for human risk assessment.

In this context, the ability of MCL to inhibit the activity of the major CYP450 isozymes was investigated. The main isozymes involved in drug metabolism were evaluated: CYP1A2, CYP2C9, CYP2C19 CYP2D6, CYP2E1, and CYP3A. The assays were performed with the racemic mixture and each single enantiomer due to the reported potential of stereoselective inhibition of CYP450 isozymes by chiral xenobiotics (Krasulova et al., 2016). Table 3 shows the MCL half-maximum inhibitory concentrations ($IC_{50}$) for each isoform and racemic mixture.

MCL (racemic mixture and single enantiomer) did not inhibit CYP1A2 or CYP2E1 ($IC_{50}$ > 100 μmol $L^{-1}$). Besides that, MCL inhibited CYP2D6 slightly ($IC_{50}$ > 80 μmol $L^{-1}$). These facts should guarantee that drugs/substrates preferentially/exclusively metabolized by these isozymes, including melatonin, caffeine, venlafaxine, and metoprolol (Sychev et al., 2018), should not have their plasma concentration altered by human exposure to MCL.

On the other hand, CYP2C9, CYP2C19, and CYP3A (Fig. 4) inhibition by MCL can lead to several cases of drug-pesticide interactions. MCL substantially inhibited the isozymes CYP2C19 and CYP3A (strong inhibition), with $IC_{50}$ lower than 4 μmol $L^{-1}$. MCL inhibited CYP2C9 less intensely ($IC_{50}$ between 26 and 36 μmol $L^{-1}$). These isozymes underlie the metabolism of more than 50% of the most commonly prescribed drugs (Sychev et al., 2018). Warfarin, S-mephenytoin, omeprazole, and quetiapine are examples of sensitive drugs metabolized by these enzymes that may have their concentration increased in the presence of a CYP450 inhibitor (Sychev et al., 2018). Therefore, patients taking these drugs could suffer a toxic effect if they have contact with MCL.

Hence, the reported exposure of the human population to MCL (Di Filippo et al., 2018; Freeman et al., 2016; Zhao et al., 2018) could lead to drug-pesticide interaction. This interaction could elicit an exacerbated increase in the drug pharmacological activity as a result of decreasing drug metabolism or toxic effect originating from a higher drug half-life in the body. Ultimately, all this could culminate in damages to the health. Zambonin et al. (2002) found a MCL concentration of 17.6 μg $kg^{-1}$ in strawberry samples, while Freeman et al. (2016) detected MCL residues (concentration higher than 0.02 ppm) in eight types of food from a total of 15 analyzed items. The acceptable MCL daily intake is 0.025 mg $kg^{-1}$ $day^{-1}$ (European Food Safety Authority, 2010). Although MCL is a moderately toxic pesticide, there is no report regarding its concentration in foods being higher than the acceptable daily intake. However, if MCL is not metabolized in the liver (as in the case of *R*-myclobutanil), it will stay longer in the human body and may

**Table 3**
$IC_{50}$ values obtained for MCL over the main CYP450 isoforms.

| CYP450 isoform | $IC_{50}$ (μmol $L^{-1}$) | | |
|---|---|---|---|
| | *rac*-MCL | *S*-(+)-MCL | *R*-(−)-MCL |
| 1A2 | > 100 | > 100 | > 100 |
| 2E1 | > 100 | > 100 | > 100 |
| 2D6 | > 100 | 81 ± 22 | 91 ± 38 |
| 2C9 | 36.3 ± 5.3 | 26.5 ± 3.7 | 31.0 ± 7.7 |
| 2C19 | 0.56 ± 0.03 | 0.29 ± 0.02 | 0.63 ± 0.05 |
| 3A[a] | 3.04 ± 0.49 | 1.19 ± 0.15 | 0.72 ± 0.05 |
| 3A[b] | 1.42 ± 0.37 | 0.58 ± 0.07 | 1.31 ± 0.27 |

Marker reaction: (a) midazolam 1-hydroxylation, (b) Nifedipine oxidation.
CYP450 - cytochrome P450.
$IC_{50}$ - half-maximal inhibitory concentration.
MCL - myclobutanil.

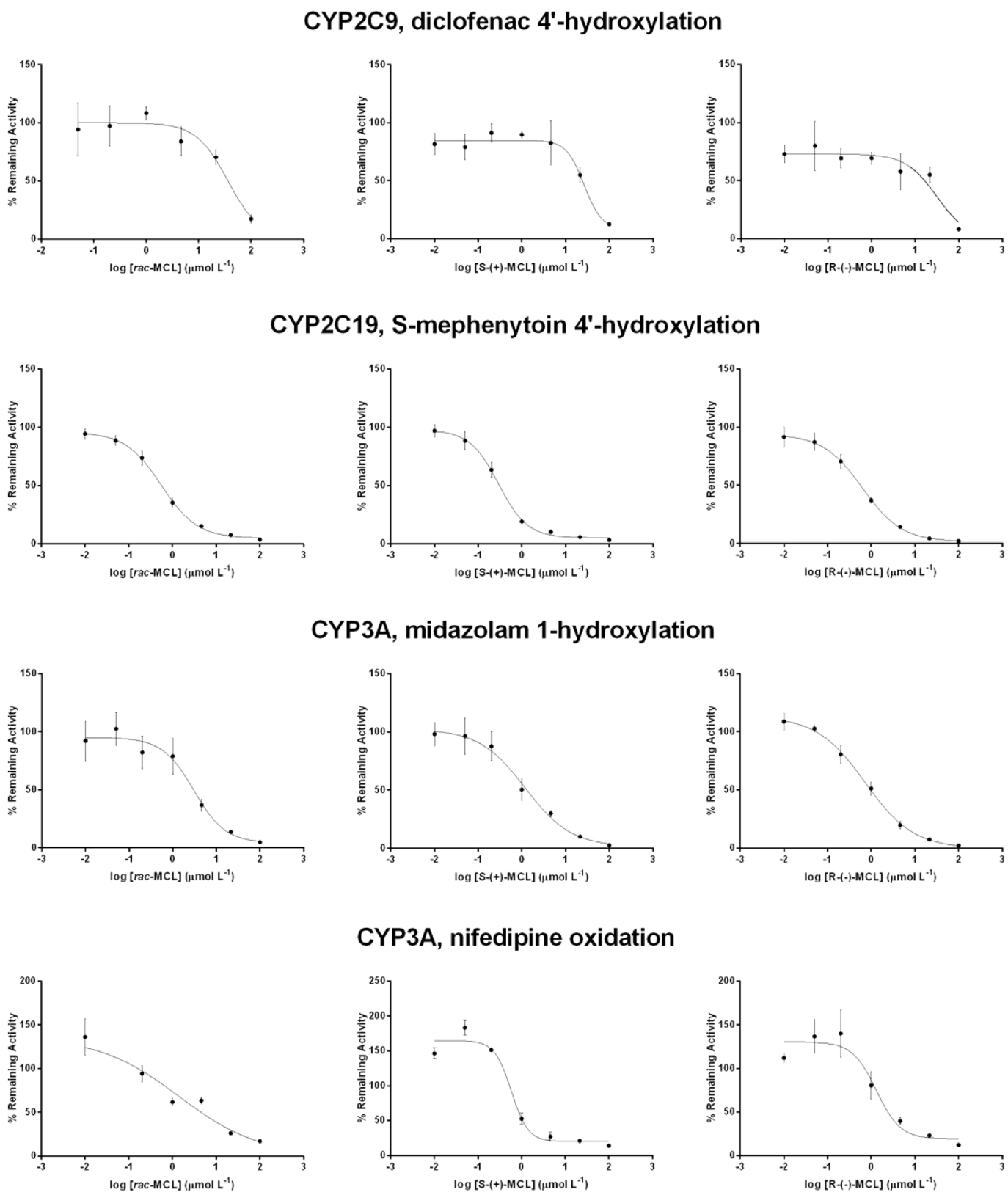


**Fig. 4.** $IC_{50}$ plots for the CYP450 enzymes inhibited by *rac*-MCL, *S*-(+)-MCL, and *R*-(−)-MCL.

cause toxic effects (i.e., it may inhibit CYP3A and CYP2C19) mainly in vulnerable people, such as children. In a controlled baby food simulation study evaluating several pesticides (Kovacova et al., 2014), myclobutanil resisted thermal degradation during household preparation of apple purée.

Although the inhibition assays did not demonstrate extensive stereoselectivity, the possibility that *R*-(−)-MCL could remain longer in the human body due to stereoselective metabolism could have significant impacts regarding CYP2C9, CYP2C19, and CYP3A inhibition in people exposed to this pesticide. A rise in *R*-(−)-MCL concentration

could lead to increasingly significant inhibitions and more severe drug-pesticide interactions. The reported enantioselective difference in MCL metabolism by CYP450 enzymes and the non-enantioselective CYP450 inhibition by MCL could be related to the different enzyme active sites for metabolism and inhibition. This difference will depend on the kind of inhibition and on the stereoselectivity; for instance, during non-competitive inhibition, the binding sites of the substrate and the inhibitor are different. Therefore, the *R*- and the *S*-enantiomers could bind to this site in the same way, while only *S*-MCL would bind to the active site and be metabolized therein.

## 4. Conclusion

The enantioselective MCL metabolism by CYP450 enzymes present in human liver microsomes has been evaluated for the first time; *rac*-MCL and the isolated enantiomers, *S*-(+)-MCL and *R*-(−)-MCL have been employed. The MCL enantiomers have significantly different metabolism: human CYP450 enzymes only metabolized the *S*-(+)-MCL enantiomer. The $V_{MAX}$ and $K_{Mapp}$ values obtained for the incubation of isolated *S*-(+)-MCL are approximately 4.6-fold and 1.9-fold higher than the $V_{MAX}$ and $K_{Mapp}$ values obtained for *rac*-MCL, respectively. The predicted *in vivo* toxicokinetic parameters indicate that *S*-(+)-myclobutanil may be preferentially eliminated by the liver and may suffer the first-pass metabolism effect. However, because CYP450 does not metabolize *R*-(−)-myclobutanil, the latter enantiomer may reach the systemic circulation, thereby remaining longer in the human body and potentially causing toxic effects. Although there are differences in the metabolism of myclobutanil enantiomers, *in vitro* inhibition studies do not show significant enantioselective differences. The studies suggest that myclobutanil can inhibit CYP2D6 and CYP2C9 moderately and CYP3A and CYP2C19 strongly. These results provide useful scientific information for myclobutanil risk assessment in humans.

## Acknowledgements

The authors are grateful to the São Paulo Research Foundation (FAPESP, grant numbers 2013/08166-5, 2014/50945-4, 2016/07597-0, 2017/03204-7, 2018/07534-4), Conselho Nacional de Desenvolvimento Científico e Tecnológico (CNPq– INCT-DATREM Process number 465571/2014-0), and Coordenação de Aperfeiçoamento de Pessoal de Nível Superior - Brasil (CAPES) - Finance Code 001, for their financial support and research fellowships.

## Appendix A. Supplementary data

Supplementary data related to this article can be found at https://doi.org/10.1016/j.fct.2019.04.009.

## Transparency document

Transparency document related to this article can be found online at https://doi.org/10.1016/j.fct.2019.04.009

## References

Abass, K., Pelkonen, O., 2013. The inhibition of major human hepatic cytochrome P450 enzymes by 18 pesticides: comparison of the N-in-one and single substrate approaches. Toxicol. Vitro 27, 1584–1588. https://doi.org/10.1016/J.TIV.2012.05.003.

Abass, K.M., 2013. From in vitro hepatic metabolic studies towards human health risk assessment: two case studies of diuron and carbosulfan. Pestic. Biochem. Physiol. 107, 258–265. https://doi.org/10.1016/J.PESTBP.2013.08.003.

Barton, H.A., Tang, J., Sey, Y.M., Stanko, J.P., Murrell, R.N., Rockett, J.C., Dix, D.J., 2006. Metabolism of myclobutanil and triadimefon by human and rat cytochrome P450 enzymes and liver microsomes. Xenobiotica 36, 793–806. https://doi.org/10.1080/00498250600821292.

Basheer, A.A., 2018. Chemical chiral pollution: impact on the society and science and need of the regulations in the 21stcentury. Chirality 30, 402–406. https://doi.org/10.1002/chir.22808.

Bowman, C.M., Benet, L.Z., 2018. An examination of protein binding and protein-facilitated uptake relating to in vitro-in vivo extrapolation. Eur. J. Pharm. Sci. 123, 502–514. https://doi.org/10.1016/j.ejps.2018.08.008.

Carrão, D.B., Gomes, I.C.R., Barbosa, F., de Oliveira, A.R.M., 2019. Evaluation of the enantioselective in vitro metabolism of the chiral pesticide fipronil employing a human model: risk assessment through in vitro-in vivo correlation and prediction of toxicokinetic parameters. Food Chem. Toxicol. 123, 225–232. https://doi.org/10.1016/J.FCT.2018.10.060.

Chang, G., Steyn, S.J., Umland, J.P., Scott, D.O., 2010. Strategic use of plasma and microsome binding to exploit in vitro clearance in early drug discovery. ACS Med. Chem. Lett. 1, 50–53. https://doi.org/10.1021/ml900012h.

Cheng, C., Di, S., Chen, L., Zhang, W., Diao, J., Zhou, Z., 2017. Enantioselective bioaccumulation, tissue distribution, and toxic effects of myclobutanil enantiomers in Pelophylax nigromaculatus tadpole. J. Agric. Food Chem. 65, 3096–3102. https://doi.org/10.1021/acs.jafc.7b00086.

Cheng, C., Huang, L., Diao, J., Zhou, Z., 2013. Enantioselective toxic effects and degradation of myclobutanil enantiomers in Scenedesmus obliquus. Chirality 25, 858–864. https://doi.org/10.1002/chir.22226.

Coleman, M.D., 2006. Introduction. In: Coleman, M.D. (Ed.), Human Drug Metabolism - an Introduction. John Wiley & Sons, Ltd, Chichester, UK, pp. 1–12. https://doi.org/10.1002/0470032669.ch1.

Damre, A.A., Iyer, K.R., 2012. The significance and determination of plasma protein binding. In: Lyubimov, A.V. (Ed.), Encyclopedia of Drug Metabolism and Interactions. John Wiley & Sons, New Jersey, pp. 1–18. https://doi.org/10.1002/9780470921920.edm032.

de Albuquerque, N.C.P., Carrão, D.B., Habenschus, M.D., de Oliveira, A.R.M., 2018. Metabolism studies of chiral pesticides: a critical review. J. Pharm. Biomed. Anal. 147, 89–109. https://doi.org/10.1016/J.JPBA.2017.08.011.

de Albuquerque, N.C.P., de Matos, J.V., de Oliveira, A.R.M., 2016. In-line coupling of an achiral-chiral column to investigate the enantioselective in vitro metabolism of the pesticide fenamiphos by human liver microsomes. J. Chromatogr. A 1467, 326–334. https://doi.org/10.1016/j.chroma.2016.08.039.

Deng, Z., Hu, J., 2011. Bioactivity investigation of fungicide myclobutanil enantiomers. Agrochemicals 50.

Di Filippo, P., Pomata, D., Riccardi, C., Buiarelli, F., De Gennaro, M., Console, C., Laurendi, V., Puri, D., 2018. Determination of pesticides in the respirable fraction of airborne particulate matter by high-performance liquid chromatography-tandem mass spectrometry. Anal. Lett. 51, 600–612. https://doi.org/10.1080/00032719.2017.1338713.

Dong, F., Cheng, L., Liu, X., Xu, J., Li, J., Li, Y., Kong, Z., Jian, Q., Zheng, Y., 2012. Enantioselective analysis of triazole fungicide myclobutanil in cucumber and soil under different application modes by chiral liquid chromatography/tandem mass spectrometry. J. Agric. Food Chem. 60, 1929–1936. https://doi.org/10.1021/jf204762t.

Drăghici, C., Chirila, E., Sica, M., 2013. Enantioselectivity of chiral pesticides in the environment. In: Simeonov, L.I., Macaev, F.Z., Simeonova, B.G. (Eds.), Environmental Security Assessment and Management of Obsolete Pesticides in Southeast Europe. Springer, Dordrecht, pp. 91–102. https://doi.org/10.1007/978-94-007-6461-3_7.

EMA, 2012. Guideline on Bioanalytical Method Validation. Eur. Med. Agency, pp. 3–23. https://doi.org/EMEA/CHMP/EWP/192217/2009.

European Food Safety Authority, 2010. Conclusion on the peer review of the pesticide risk assessment of the active substance myclobutanil. EFSA J. 8, 1682. https://doi.org/10.2903/jefsa.2010.1682.

Freeman, S., Kaufman-Shriqui, V., Berman, T., Varsano, R., Shahar, D.R., Manor, O., 2016. Children's diets, pesticide uptake, and implications for risk assessment: an Israeli case study. Food Chem. Toxicol. 87, 88–96. https://doi.org/10.1016/J.FCT.2015.11.009.

Giuliano, C., Jairaj, M., Zafiu, C.M., Laufer, R., 2005. Direct determination of unbound intrinsic drug clearance in the microsomal stability assay. Drug Metab. Dispos. 33, 1319–1324. https://doi.org/10.1124/dmd.105.005033.

Godin, S.J., Crow, J.A., Scollon, E.J., Hughes, M.F., DeVito, M.J., Ross, M.K., 2007. Identification of rat and human cytochrome P450 isoforms and a rat serum esterase that metabolize the pyrethroid insecticides deltamethrin and esfenvalerate. Drug Metab. Dispos. 35, 1664–1671. https://doi.org/10.1124/dmd.107.015388.

Habenschus, M.D., Moreira, F.D.L., Lopes, N.P., De Oliveira, A.R.M., 2017. In vitro inhibition of human CYP450s 1A2, 2C9, 3A4/5, 2D6 and 2E1 by grandisin. Planta Med. 83, 727–736. https://doi.org/10.1055/s-0042-124615.

Hao, W., Hu, X., Zhu, F., Chang, J., Li, J., Li, W., Wang, H., Guo, B., Li, J., Xu, P., Zhang, Y., 2018. Enantioselective distribution, degradation, and metabolite formation of myclobutanil and transcriptional responses of metabolic-related genes in rats. Environ. Sci. Technol. 52, 8830–8837. https://doi.org/10.1021/acs.est.8b01721.

Kovacova, J., Kocourek, V., Kohoutkova, J., Lansky, M., Hajslova, J., 2014. Production of apple-based baby food: changes in pesticide residues. Food Addit. Contam. A 31, 1089–1099. https://doi.org/10.1080/19440049.2014.912356.

Krasulova, K., Siller, M., Holas, O., Dvorak, Z., Anzenbacher, P., 2016. Enantiospecific effects of chiral drugs on cytochrome P450 inhibition in vitro. Xenobiotica 46, 315–324. https://doi.org/10.3109/00498254.2015.1076086.

Li, Y., Dong, F., Liu, X., Xu, J., Han, Y., Zheng, Y., 2015. Enantioselectivity in tebuconazole and myclobutanil non-target toxicity and degradation in soils. Chemosphere 122, 145–153. https://doi.org/10.1016/j.chemosphere.2014.11.031.

Lin, C., Zhang, L., Zhang, H., Wang, Q., Zhu, J., Wang, J., Qian, M., 2018. Enantioselective degradation of myclobutanil and famoxadone in grape. Environ. Sci. Pollut. Res. 25, 2718–2725. https://doi.org/10.1007/s11356-017-0539-4.

Liu, W., Tang, M., 2011. Enantioselective activity and toxicity of chiral herbicides. In: Hasaneen, M.N. (Ed.), Herbicides - Mechanisms and Mode of Action. InTech, pp. 63–80. https://doi.org/10.5772/33179.

Martignoni, M., Groothuis, G.M.M., de Kanter, R., 2006. Species differences between mouse, rat, dog, monkey and human CYP-mediated drug metabolism, inhibition and induction. Expert Opin. Drug Metabol. Toxicol. 2, 875–894. https://doi.org/10.1517/17425255.2.6.875.

Mazur, C.S., Kenneke, J.F., Tebes-Stevens, C., Okino, M.S., Lipscomb, J.C., 2007. In vitro metabolism of the fungicide and environmental contaminant trans-bromuconazole and implications for risk assessment. J. Toxicol. Environ. Health Part A Curr. Issues 70, 1241–1250. https://doi.org/10.1080/15287390701380914.

Neese, F., 2012. The ORCA program system. WIREs Comput. Mol. Sci. 2, 73–78. https://doi.org/10.1002/wcms.81.

Ogilvie, B.W., Usuki, E., Phyllis, Y., Parkinson, A., 2008. In vitro approaches for studying the inhibition of drug-metabolizing enzymes and identifying the drug-metabolizing enzymes responsible for the metabolism of drugs (reaction phenotyping) with emphasis on cytochrome P450. In: Rodrigues, A.D. (Ed.), Drug-Drug Interactions. Informa Healthcare.

Pedretti, A., Villa, L., Vistoli, G., 2004. VEGA - an open platform to develop chemo-bioinformatics applications, using plug-in architecture and script programming. J. Comput. Aided Mol. Des. 18, 167–173. https://doi.org/10.1023/B:JCAM.0000035186.90683.f2.

Pedretti, A., Villa, L., Vistoli, G., 2003. Atom-type description language: a universal language to recognize atom types implemented in the VEGA program. Theor. Chem. Accounts Theor. Comput. Model. 109, 229–232. https://doi.org/10.1007/s00214-002-0402-6.

Pedretti, A., Villa, L., Vistoli, G., 2002. VEGA: a versatile program to convert, handle and visualize molecular structure on windows-based PCs. J. Mol. Graph. Model. 21, 47–49.

Ring, B., Wrighton, S.A., Mohutsky, M., 2014. Reversible mechanisms of enzyme inhibition and resulting clinical significance. In: Nagar, S., Argikar, U.A., Tweedie, D.J. (Eds.), Enzyme Kinetics in Drug Metabolism: Fundamentals and Applications. Humana Press, New York, pp. 37–56. https://doi.org/10.1007/978-1-62703-758-7_4.

Rodrigues, A.D., 1999. Integrated cytochrome P450 reaction phenotyping. Attempting to bridge the gap between cDNA-expressed cytochromes P450 and native human liver microsomes. Biochem. Pharmacol. 57, 465–480. https://doi.org/10.1016/S0006-2952(98)00268-8.

Seibert, E., Tracy, T.S., 2014. Fundamentals of enzyme kinetics. In: Nagar, S., Argikar, U.A., Tweedie, D.J. (Eds.), Enzyme Kinetics in Drug Metabolism: Fundamentals and Applications. Humana Press, New York, pp. 9–22. https://doi.org/10.1007/978-1-62703-758-7_2.

Sun, M., Liu, D., Qiu, X., Zhou, Q., Shen, Z., Wang, P., Zhou, Z., 2014. Acute toxicity, bioactivity, and enantioselective behavior with tissue distribution in rabbits of myclobutanil enantiomers. Chirality 26, 784–789. https://doi.org/10.1002/chir.22353.

Sychev, D.A., Ashraf, G.M., Svistunov, A.A., Maksimov, M.L., Tarasov, V.V., Chubarev, V.N., Otdelenov, V.A., Denisenko, N.P., Barreto, G.E., Aliev, G., 2018. The cytochrome P450 isoenzyme and some new opportunities for the prediction of negative drug interaction in vivo. Drug Des. Dev. Ther. 12, 1147–1156. https://doi.org/10.2147/DDDT.S149069.

University of Hertfordshire, 2018. Pesticide Properties DataBase - Myclobutanil. (WWW Document).

Wang, Y., Qiu, J., Zhu, W., Wang, X., Zhang, P., Wang, D., Zhou, Z., 2015. Enantioselective metabolism and interference on tryptophan metabolism of myclobutanil in rat hepatocytes. Chirality 27, 643–649. https://doi.org/10.1002/chir.22479.

Yan, J., Zhang, P., Wang, X., Wang, Y., Zhou, Z., Zhu, W., 2014. Stereoselective degradation of chiral fungicide myclobutanil in rat liver microsomes. Chirality 26, 51–55. https://doi.org/10.1002/chir.22265.

Yao, Z., Qian, M., Zhang, H., Nie, J., Ye, J., Li, Z., 2016. Etoxazole is metabolized enantioselectively in liver microsomes of rat and human in vitro. Environ. Sci. Technol. 50, 9682–9688. https://doi.org/10.1021/acs.est.6b02676.

Zambonin, C.G., Cilenti, A., Palmisano, F., 2002. Solid-phase microextraction and gas chromatography – mass spectrometry for the rapid screening of triazole residues in wine and strawberries. J. Chromatogr. A 967, 255–260. https://doi.org/10.1016/S0021-9673(02)00780-X.

Zhang, H., Wang, X., Qian, M., Wang, X., Xu, H., Xu, M., Wang, Q., 2011. Residue analysis and degradation studies of fenbuconazole and myclobutanil in strawberry by chiral high-performance liquid chromatography-tandem mass spectrometry. J. Agric. Food Chem. 59, 12012–12017. https://doi.org/10.1021/jf202975x.

Zhao, P., Lei, S., Xing, M., Xiong, S., Guo, X., 2018. Simultaneous enantioselective determination of six pesticides in aqueous environmental samples by chiral liquid chromatography with tandem mass spectrometry. J. Sep. Sci. 41, 1287–1297. https://doi.org/10.1002/jssc.201701259.